JOURNAL OF THERMOPHYSICS AND HEAT TRANSFER
Vol. 24, No. 4, October–December 2010

Thermodynamic Analysis of Slip Flow Forced Convection Through a Microannulus

Arman Sadeghi,* Abolhassan Asgarshamsi,† and Mohammad Hassan Saidi‡
Sharif University of Technology, 11365 Tehran, Iran

DOI: 10.2514/1.48036

The present investigation is devoted to the second law of thermodynamics analysis of steady-state hydrodynamically and thermally fully developed laminar gas flow in a microannulus with constant but different wall heat fluxes. Slip velocity and temperature jump boundary conditions are used to describe rarefaction effects. Viscous heating is also included for both the wall cooling and heating cases. Using already available velocity profile, closed-form expressions are obtained for the transverse distribution of temperature and entropy generation rates. The results demonstrate that the effect of the wall heat fluxes ratio on entropy generation is negligible at large values of the group parameter and Peclet number, while the effect of increasing values of the annulus geometrical aspect ratio is to severely increase entropy generation. The entropy generation decreases as Knudsen and Peclet numbers increase, however, the effect of increasing Brinkman number and the group parameter is to increase entropy generation. Furthermore, it is realized that the influences of rarefaction on entropy generation are slighter for low Peclet number flows.

Nomenclature

Be	=	Bejan number, N_{HT}/N_S
Br	=	Brinkman number, $\mu U^2/(q_i + q_o)r_o$
c_p	=	specific heat at constant pressure, kJ kg^{-1} K^{-1}
D_h	=	hydraulic diameter of channel, $2(r_o - r_i)$
F_m	=	momentum accommodation coefficient
F_t	=	thermal accommodation coefficient
h	=	heat transfer coefficient, Wm^{-2} K^{-1}
Kn	=	Knudsen number, λ/D_h
k	=	thermal conductivity, Wm^{-1} K^{-1}
N_{FF}	=	entropy generation number related to fluid friction
N_{HT}	=	entropy generation number related to heat transfer
N_S	=	entropy generation number, total, $S_G/S_{G,C}$
$N_{S,\mathrm{av}}$	=	average entropy generation number
n	=	normal direction exiting the wall, m
Pe	=	Peclet number, $RePr$
Pr	=	Prandtl number, ν/α
p	=	pressure, Pa
q	=	heat flux, Wm^{-2}
Re	=	Reynolds number, UD_h/ν
r	=	radial coordinate, m
r^*	=	dimensionless radial coordinate, r/r_o
r_m	=	the radius where the maximum velocity occurs, m
r_m^*	=	dimensionless form of r_m, r_m/r_o
S_G	=	entropy generation rate, Wm^{-3} K^{-1}
$S_{G,C}$	=	characteristic entropy generation rate, Wm^{-3} K^{-1}
T	=	temperature, K
U	=	mean velocity, ms^{-1}
u	=	axial velocity, ms^{-1}
u^*	=	dimensionless axial velocity, u/U
x	=	axial coordinate, m

Greek symbols

α	=	thermal diffusivity, m^2 s^{-1}
β	=	annulus aspect ratio, r_i/r_o
γ	=	heat capacity ratio
η	=	wall heat fluxes ratio, q_o/q_i
θ	=	dimensionless temperature, Eq. (12)
θ^*	=	dimensionless temperature, Eq. (26)
λ	=	gas mean free path, m
μ	=	dynamic viscosity, kgm^{-1} s^{-1}
ν	=	kinematic viscosity, m^2 s^{-1}
Ω	=	dimensionless temperature difference, $(q_i + q_o)r_o/kT_0$

Subscripts

b	=	bulk
c	=	critical
i	=	inner wall
o	=	outer wall
s	=	fluid properties at solid surface
w	=	wall
0	=	reference

Received 7 November 2009; revision received 7 April 2010; accepted for publication 10 April 2010.

*Ph.D. Student, Center of Excellence in Energy Conversion (CEEC), School of Mechanical Engineering, P.O. Box 11155-9567; armansadeghi@mech.sharif.ir.

†Ph.D. Student, CEEC, School of Mechanical Engineering, P.O. Box 11155-9567; a_shamsi@mech.sharif.ir.

‡Professor, CEEC, School of Mechanical Engineering, P.O. Box 11155-9567; saman@sharif.edu.

I. Introduction

THROUGH the past two decades, fluid flow and heat transfer in microchannels have been attractive research fields due to the rapid development of microelectromechanical systems and other microscale devices such as integrated circuits and biochemical systems. The hydraulic diameter of a microchannel is typically within 1 and 100 μm. This characteristic geometric scale is comparable with the gas mean free path in which at standard atmospheric condition is about 100 nm. In this case, the gas flow cannot be modeled based on the continuum hypothesis since the rarefaction effects are significant. The gas status deviation from continuum behavior is measured by the Knudsen number Kn, which is defined as $Kn = \lambda/D_h$, where λ is the mean free path of gas molecules and D_h is the channel hydraulic diameter. Based on a definition given by Beskok and Karniadakis [1], gas flow can be classified as one of four regimes according to its Knudsen number. In the slip flow regime which corresponds to $10^{-3} \leq Kn \leq 0.1$, deviations from the state of continuum are relatively small and the Navier–Stokes equations are still valid. The rarefaction effect can be modeled through the partial slip at the wall using slip boundary conditions which can be determined using kinetic theory of gases. The experiments conducted by Liu et al. [2]

and Hsieh et al. [3] on the transport of gases through microchannels confirm that Navier–Stokes equations subject to first order slip boundary conditions can be used to obtain flow characteristics in micron-size devices.

Hydrodynamic aspects of slip flow in the circular tube and parallel plate channel was studied by Kennard [4]. Ebert and Sparrow [5] have determined the velocity distribution and pressure drop of slip flow in rectangular and annular ducts. More recently, Duan and Muzychka [6] have performed an analytical analysis to describe fully developed laminar flow in elliptical microchannels. The method of eigenfunction expansion and collocation was used by Wang [7] in order to solve the velocity distribution for slip flow in ducts of polygonal, elliptic and cuspidal cross sections. Bahrami et al. [8] developed a compact approximate model to determine the pressure drop of slip flow through arbitrary cross-sectional microchannels. The comprehensive results taken from [4–8], which are related to fully developed condition, show that for a given mass flow rate, rarefaction effect decreases pressure drop in microchannels compared with conventional channels. Zhang et al. [9] provided an analytical solution for velocity distribution of developing slip flow in a parallel plate microchannel, using the homotopy analysis method. They have also performed a numerical simulation in order to study hydrodynamic aspects of three-dimensional compressible gaseous slip flow in rectangular microchannels [10].

Slip flow forced convection in microchannels of different cross section has been extensively investigated in the literature. The problem of laminar slip flow forced convection in microtubes with uniform wall heat flux has been analytically studied by Ameel et al. [11]. They showed that as Knudsen number increases the fully developed Nusselt number decreases. Zhu et al. [12] performed a theoretical analysis for slip flow heat transfer in a parallel plate microchannel with constant but different wall heat fluxes. The analysis was accomplished by combining the solutions of two sub problems consisting of a microchannel with one wall being adiabatic and the other having constant heat flux. Recently, Zhang et al. [13] have extended the work of Zhu et al. [12] by taking into account the effects of viscous heating. Duan and Muzychka [14] have studied heat transfer characteristics of fully developed laminar rarefied gas flow in annular microducts with constant wall heat fluxes, neglecting viscous heating effects. Avci and Aydin [15] analytically studied slip flow heat transfer in a microannulus for the special case of one wall being adiabatic and the other having constant heat flux, considering viscous heating effects. Tunc and Bayazitoglu [16] have studied both hydrodynamically- and thermally-fully developed slip flow in rectangular microducts having constant wall heat flux, using integral transform method. Hooman [17] proposed a superposition approach to investigate forced convection in microducts of arbitrary cross section, subject to H1 and H2 boundary conditions, in the slip flow regime. Fresh theoretical analysis of slip flow forced convection in a microchannel of triangular cross section was presented to put emphasis on the applicability of the proposed approach. Analytical modeling of fluid flow and heat transfer in microchannel/nanochannel heat sinks has been carried out by Khan and Yovanovich [18]. It was demonstrated that friction factor and Nusselt number decrease with increase in Knudsen number and channel aspect ratio. Based on perturbation techniques, closed-form solutions were presented by Hooman et al. [19] for slip flow forced convection of a gas with temperature-dependent properties in a microchannel with the effects of viscous dissipation being included. In a recent study, Sadeghi et al. [20] performed a boundary layer analysis for simultaneously developing flow through parallel plate microchannels in order to determine the effects of Knudsen number on friction factor, Nusselt number and entry length.

In comparison with forced convection, less attention has been given to free convection slip flow in the literature. The first work in this field has been done by Chen and Weng [21], which analytically studied fully developed natural convection in an open-ended vertical parallel plate microchannel with asymmetric wall temperature distributions. They afterwards extended their works by taking the effects of thermal creep [22] and variable physical properties [23] into account. Natural convection gaseous slip flow in a vertical parallel plate microchannel with isothermal wall conditions was numerically investigated by Biswal et al. [24], in order to analyze the influence of the entrance region on the overall heat transfer characteristics. Chakraborty et al. [25] performed a boundary layer integral analysis to investigate the heat transfer characteristics of natural convection gas flow in symmetrically heated vertical parallel plate microchannels. It was revealed that for low Rayleigh numbers, the entrance length is only a small fraction of the total channel extent.

Entropy generation plays an important role in the design and development of thermofluid components. Entropy generation, which in the flow systems is due to fluid friction and heat transfer, destroys available work of the system. Bejan [26,27] focused on the different reasons behind entropy generation in applied thermal engineering. He showed that entropy minimization improves system efficiency. To better understand the significance of entropy minimization in the design of thermofluid systems a practical example will be helpful. A common design problem in microelectronics is the efficient design of a cooling system for microprocessors, where by efficient we mean the condition in which the system requires minimum pumping power requirement to overcome the fluid friction, while still conveying the total heat generated in the system. For this system, the point of minimum entropy production corresponds to the condition in which the ratio of heat transfer to the pumping power is maximum.

Although there are numerous works related to second law analysis of macroscale devices, unfortunately the open literature shows very small number of papers dealing with entropy generation in microdevices. Haddad et al. [28] were the first who performed the second law analysis for a microchannel. They numerically investigated the entropy generation due to developing laminar forced convection through parallel plate microchannels. Avci and Aydin [29] have performed the second law analysis for microtube and parallel plate microchannel considering constant wall heat flux. Hooman [30] presented closed-form solutions for fully developed temperature distribution and entropy generation due to forced convection in two above mentioned cross sections for two different thermal boundary conditions, saying isothermal and isoflux walls. Yari [31] investigated the entropy generation in a microannulus with one wall being adiabatic and the other having constant heat flux. Fully developed laminar flow at high Peclet number was considered and the viscous dissipation effect was taken into consideration. Numerical techniques were used to determine entropy generation rates, using the previously obtained velocity and temperature distributions.

Microannulus is a useful type of microchannels which can be used as a micro heat exchanger. Such a geometry can also be found in cooling of high power resistive magnets, compact fission reactor cores, fusion reactor blankets, advanced space thermal management systems and high density multi chip modules in supercomputers and other modular electronics [32]. The only work dealing with the second law analysis of a microannulus, performed by Yari [31] was based on quite strong assumptions such as neglecting the axial variation of temperature and assuming one wall to be adiabatic. In real microfluidic applications, the Reynolds number is relatively small, so neglecting the axial variation of temperature may lead to a large amount of error in evaluating entropy generation rates. Furthermore, since numerical techniques were used to determine entropy generation rates, just the results of the perfect accommodation of gas on the surface are available. In the present study, we intend to remove the above assumptions by investigating the entropy generation in fully developed forced convection in a microannulus with asymmetric constant heat flux boundary condition which may cover most of the practical microflow boundary conditions. Viscous heating is included in the analysis and the rarefaction effects are taken into consideration using first order slip boundary conditions. Using already available velocity distribution, the energy equation is solved to get the temperature distribution analytically and consequently to compute the entropy generation rates.

II. Problem Formulation

A. Slip Velocity and Temperature Jump

As mentioned earlier, because of the slip conditions, fluid particles adjacent to solid surface no longer attain the velocity and temperature of the solid surface. Therefore, the fluid particles have a tangential velocity which is the slip velocity and a finite temperature difference which is temperature jump, at the solid boundary. Using first order slip boundary conditions, the slip velocity and temperature jump are, respectively, expressed as [33]

$$u_s = \frac{2-F_m}{F_m} KnD_h \left(\frac{\partial u}{\partial n}\right)_w \tag{1}$$

$$T_s - T_w = \frac{2-F_t}{F_t}\frac{2\gamma}{1+\gamma}\frac{KnD_h}{Pr}\left(\frac{\partial T}{\partial n}\right)_w \tag{2}$$

where u_s and T_s are the velocity and temperature of the gas at the wall, respectively, T_w is the wall temperature, n is the normal direction exiting the wall, F_m is the tangential momentum accommodation coefficient and F_t is the thermal accommodation coefficient.

The accommodation coefficients depend on various parameters that affect surface interaction, such as the magnitude and the direction of the velocity. It is shown that these coefficients are reasonably constant for a given gas and surface combination [34]. For light gases the accommodation coefficients may differ significantly from unity, while for heavy gases they are close to unity. If one deals with a sufficiently heavy gas and an ordinarily contaminated surface, one may assume the values of accommodation coefficients to be one [35]. According to Hadjiconstantinou [36], for most engineering applications the values of accommodation coefficients are close to unity.

B. Hydrodynamic Aspects

The geometry of physical problem is shown in Fig. 1. Flow is considered to be steady, hydrodynamically-fully developed and having constant properties. Using cylindrical coordinates, the momentum equation in the x-direction and relevant boundary conditions are

$$\frac{1}{r}\frac{\mathrm{d}}{\mathrm{d}r}\left(r\frac{\mathrm{d}u}{\mathrm{d}r}\right) = \frac{1}{\mu}\frac{\mathrm{d}p}{\mathrm{d}x} = \text{const.} \tag{3}$$

$$\begin{aligned} u_{(r_i)} &= \frac{2-F_m}{F_m} KnD_h \left(\frac{\mathrm{d}u}{\mathrm{d}r}\right)_{(r_i)} \\ u_{(r_o)} &= -\frac{2-F_m}{F_m} KnD_h \left(\frac{\mathrm{d}u}{\mathrm{d}r}\right)_{(r_o)} \end{aligned} \tag{4}$$

in which $D_h = 2(r_o - r_i)$. Using the following dimensionless parameters

$$r^* = \frac{r}{r_o}, \qquad \beta = \frac{r_i}{r_o}, \qquad u^* = \frac{u}{U} \tag{5}$$

where U is the mean velocity, the dimensionless velocity distribution is [15]

$$u^* = (1 - r^{*2} + 2r_m^{*2}\,\ell_n\, r^* + A)/B \tag{6}$$

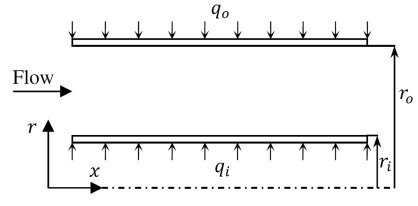

Fig. 1 Schematic diagram of the problem.

where A and B are as follows:

$$A = 4(1-\beta)(1-r_m^{*2})\frac{2-F_m}{F_m}Kn \tag{7}$$

$$B = \frac{1}{2}\left[1 - \beta^2 - 4r_m^{*2}\left(\frac{1}{2} + \frac{\beta^2}{1-\beta^2}\,\ell_n\,\beta\right) + 2A\right] \tag{8}$$

in which r_m^* represents the dimensionless radius where the maximum velocity occurs ($\mathrm{d}u/\mathrm{d}r = 0$). It is given by

$$r_m^* = \frac{r_m}{r_o} = \left[\frac{(1-\beta^2)(1+4\frac{2-F_m}{F_m}Kn)}{2\,\ell_n(1/\beta) - 4\frac{2-F_m}{F_m}Kn(\frac{\beta^2-1}{\beta})}\right]^{1/2} \tag{9}$$

C. First Law Analysis

Besides the assumptions that have been done so far, for convenience of analysis, flow is considered to be thermally-fully developed. The outer and inner wall heat fluxes are assumed to be constant and different from each other, given by q_o and q_i, respectively. The directions of heat fluxes are positive while they are towards the fluid, otherwise they are negative. The conservation of energy including the effect of the viscous dissipation requires

$$u\frac{\partial T}{\partial x} = \alpha\left[\frac{\partial^2 T}{\partial x^2} + \frac{1}{r}\frac{\partial}{\partial r}\left(r\frac{\partial T}{\partial r}\right)\right] + \frac{\nu}{c_p}\left(\frac{\mathrm{d}u}{\mathrm{d}r}\right)^2 \tag{10}$$

and relevant boundary conditions are

$$\begin{aligned} T_{(r_i)} - T_{wi} &= \frac{2-F_t}{F_t}\frac{2\gamma}{1+\gamma}\frac{KnD_h}{Pr}\left(\frac{\partial T}{\partial r}\right)_{(r_i)} \\ \text{or} \quad -k\left(\frac{\partial T}{\partial r}\right)_{(r_i)} &= q_i \\ T_{(r_o)} - T_{wo} &= -\frac{2-F_t}{F_t}\frac{2\gamma}{1+\gamma}\frac{KnD_h}{Pr}\left(\frac{\partial T}{\partial r}\right)_{(r_o)} \\ \text{or} \quad k\left(\frac{\partial T}{\partial r}\right)_{(r_o)} &= q_o \end{aligned} \tag{11}$$

The dimensionless temperature θ is introduced in the following which is only dependent on r for fully developed flow:

$$\theta(r) = \frac{T - T_{so}}{\frac{(q_i+q_o)r_o}{k}} \tag{12}$$

Taking differentiation of Eq. (12) with respect to x gives

$$\frac{\partial T}{\partial x} = \frac{\mathrm{d}T_{so}}{\mathrm{d}x} = \frac{\mathrm{d}T_b}{\mathrm{d}x} = \text{const.} \tag{13}$$

in which T_b is the bulk temperature. From an energy balance on a length of duct $\mathrm{d}x$, the following expression is obtained for $\mathrm{d}T_b/\mathrm{d}x$:

$$\frac{\mathrm{d}T_b}{\mathrm{d}x} = \frac{2(r_i q_i + r_o q_o)}{\rho c_p U(r_o^2 - r_i^2)} + 8\frac{\mu U}{B^2 \rho c_p r_o^2}\left(\frac{1+\beta^2}{4} - r_m^{*4}\frac{\ell_n\,\beta}{1-\beta^2} - r_m^{*2}\right) \tag{14}$$

Since $\partial T/\partial x$ is constant, the axial conduction term in the energy equation will be zero. The energy equation then is modified into the following dimensionless form:

$$\frac{1}{r^*}\frac{\mathrm{d}}{\mathrm{d}r^*}\left(r^*\frac{\mathrm{d}\theta}{\mathrm{d}r^*}\right) = a - br^{*2} - \frac{c}{r^{*2}} + d\,\ell_n\, r^* \tag{15}$$

where a, b, c and d are as follows:

$$a = \frac{1+A}{B}\left[\frac{2(\beta+\eta)}{(1+\eta)(1-\beta^2)} + 8\frac{Br}{B^2}\left(\frac{1+\beta^2}{4} - r_m^{*4}\frac{\ell_n\,\beta}{1-\beta^2} - r_m^{*2}\right)\right] + 8\frac{Br}{B^2}r_m^{*2} \tag{16}$$

$$b = \frac{1}{B}\left[\frac{2(\beta+\eta)}{(1+\eta)(1-\beta^2)} + 8\frac{Br}{B^2}\left(\frac{1+\beta^2}{4} - r_m^{*4}\frac{\ell_n\,\beta}{1-\beta^2} - r_m^{*2}\right)\right] + 4\frac{Br}{B^2} \tag{17}$$

$$c = 4\frac{Br}{B^2}r_m^{*4} \tag{18}$$

$$d = 2\frac{r_m^{*2}}{B}\left[\frac{2(\beta+\eta)}{(1+\eta)(1-\beta^2)} + 8\frac{Br}{B^2}\left(\frac{1+\beta^2}{4} - r_m^{*4}\frac{\ell_n\,\beta}{1-\beta^2} - r_m^{*2}\right)\right] \tag{19}$$

where $\eta = q_o/q_i$ and Br is the Brinkman number given by

$$Br = \frac{\mu U^2}{(q_i+q_o)r_o} \tag{20}$$

The thermal boundary conditions in the dimensionless form are written as

$$\left(\frac{\mathrm{d}\theta}{\mathrm{d}r^*}\right)_{(\beta)} = -\frac{1}{1+\eta}, \qquad \theta_{(1)} = 0 \tag{21}$$

Using Eq. (15) and applying boundary conditions (21), the dimensionless temperature distribution is obtained as

$$\theta(r^*) = \frac{a}{4}r^{*2} - \frac{b}{16}r^{*4} - \frac{c}{2}(\ell_n\,r^*)^2 + \frac{d}{4}(r^{*2}\,\ell_n\,r^* - r^{*2}) + e\,\ell_n\,r^* + f \tag{22}$$

where e and f are as follows:

$$e = -\frac{a}{2}\beta^2 + \frac{b}{4}\beta^4 + c\,\ell_n\,\beta - \frac{d}{4}(2\beta^2\,\ell_n\,\beta - \beta^2) - \frac{\beta}{1+\eta} \tag{23}$$

$$f = -\frac{a}{4} + \frac{b}{16} + \frac{d}{4} \tag{24}$$

Equation (22) which is in terms of T_{so} can be transformed into the equation in terms of T_{wo}, using the following conversion formula

$$\frac{T_{wo}-T_{so}}{\frac{(q_i+q_o)r_o}{k}} = \frac{2-F_t}{F_t}\frac{4\gamma}{1+\gamma}\frac{\eta}{1+\eta}\frac{Kn}{Pr}(1-\beta) \tag{25}$$

So that Eq. (22) becomes

$$\theta^*(r^*) = \frac{T-T_{wo}}{\frac{(q_i+q_o)r_o}{k}} = \frac{T-T_{so}}{\frac{(q_i+q_o)r_o}{k}} - \frac{T_{wo}-T_{so}}{\frac{(q_i+q_o)r_o}{k}}$$
$$= \frac{a}{4}r^{*2} - \frac{b}{16}r^{*4} - \frac{c}{2}(\ell_n\,r^*)^2 + \frac{d}{4}(r^{*2}\,\ell_n\,r^* - r^{*2}) + e\,\ell_n\,r^* + f - \frac{2-F_t}{F_t}\frac{4\gamma}{1+\gamma}\frac{\eta}{1+\eta}\frac{Kn}{Pr}(1-\beta) \tag{26}$$

It is noteworthy that when the inner wall is adiabatic ($\eta \to \infty$), our definition for nondimensional temperature is identical to that of Avci and Aydin [15] and both results are in quite agreement.

D. Second Law Analysis

Entropy is generated due to the presence of irreversibility, and entropy generation is adopted as a quantitative measure of the irreversibility associated with a process. Flow and heat transfer processes are irreversible inside the microchannel. The nonequilibrium conditions arise due to the exchange of energy and momentum within the fluid and at solid boundaries, thus resulting in entropy generation. Part of entropy production is due to heat transfer in the direction of finite temperature gradients and other part of entropy production arises due to the fluid friction. According to Bejan [37], the volumetric rate of entropy generation can be derived as

$$S_G = \frac{k}{T_0^2}\left[\left(\frac{\partial T}{\partial x}\right)^2 + \left(\frac{\partial T}{\partial r}\right)^2\right] + \frac{\mu}{T_0}\left(\frac{\mathrm{d}u}{\mathrm{d}r}\right)^2 \tag{27}$$

where T_0 is the absolute reference temperature. In writing Eq. (27) the assumption was made that the temperature variation over the channel cross section is negligible compared with the absolute temperature. Equation (27) can be made dimensionless to get entropy generation number N_S as

$$N_S = \frac{S_G}{S_{G,C}} = \left\{\frac{4(1-\beta)^2}{Pe^2}\left[\frac{2(\beta+\eta)}{(1+\eta)(1-\beta^2)} + 8\frac{Br}{B^2}\left(\frac{1+\beta^2}{4} - r_m^{*4}\frac{\ell_n\,\beta}{1-\beta^2} - r_m^{*2}\right)\right]^2 + \left(\frac{\mathrm{d}\theta^*}{\mathrm{d}r^*}\right)^2\right\} + \frac{Br}{\Omega}\left(\frac{\mathrm{d}u^*}{\mathrm{d}r^*}\right)^2 = N_{\mathrm{HT}} + N_{\mathrm{FF}} \tag{28}$$

where the dimensionless temperature difference Ω and the characteristic entropy generation rate $S_{G,C}$ are given by

$$\Omega = \frac{(q_i+q_o)r_o}{kT_0} \tag{29}$$

$$S_{G,C} = \frac{(q_i+q_o)^2}{kT_0^2} \tag{30}$$

The ratio of Brinkman number to dimensionless temperature difference Br/Ω is known as the group parameter. The group parameter is an important dimensionless number for irreversibility analysis. It measures the importance of viscous effects and cannot be neglected in real flow situations [27]. On the right-hand side of Eq. (28), N_{HT} represents entropy generation due to heat transfer and N_{FF} is the fluid friction contribution to entropy generation. Using dimensionless velocity and temperature distributions given by Eqs. (6) and (26), respectively, entropy generation number becomes

$$N_S = \frac{4(1-\beta)^2}{Pe^2}\left[\frac{2(\beta+\eta)}{(1+\eta)(1-\beta^2)} + 8\frac{Br}{B^2}\left(\frac{1+\beta^2}{4} - r_m^{*4}\frac{\ell_n\,\beta}{1-\beta^2} - r_m^{*2}\right)\right]^2 + \left[\frac{a}{2}r^* - \frac{b}{4}r^{*3} - \frac{c}{r^*}\ell_n\,r^* + \frac{d}{4}r^*(2\,\ell_n\,r^* - 1) + \frac{e}{r^*}\right]^2 + \frac{4}{B^2}\frac{Br}{\Omega}\left(r^* - \frac{r_m^{*2}}{r^*}\right)^2 \tag{31}$$

The average dimensionless entropy generation over the cross section of the microchannel can be computed by the following integration:

$$N_{S,\mathrm{av}} = \frac{\int_\beta^1 N_S r^*\,\mathrm{d}r^*}{\int_\beta^1 r^*\,\mathrm{d}r^*} = \frac{2}{1-\beta^2}\int_\beta^1 N_S r^*\,\mathrm{d}r^* \tag{32}$$

By integration, the average dimensionless entropy generation is obtained as follows:

$$N_{S,\mathrm{av}} = \frac{4(1-\beta)^2}{Pe^2}\left[\frac{2(\beta+\eta)}{(1+\eta)(1-\beta^2)} + 8\frac{Br}{B^2}\left(\frac{1+\beta^2}{4} - r_m^{*4}\frac{\ell_n\beta}{1-\beta^2} - r_m^{*2}\right)\right]^2 + ae - \frac{de}{2} - \frac{8}{B^2}\frac{Br}{\Omega}r_m^{*2} + \frac{1+\beta^2}{2}\left(\frac{a^2}{4}+\frac{d^2}{16}-\frac{ad}{4}-\frac{be}{2}+\frac{4}{B^2}\frac{Br}{\Omega}\right) + \frac{2}{1-\beta^2}\left\{\frac{1-\beta^6}{6}\left(\frac{bd}{8}-\frac{ab}{4}\right)+\frac{1-\beta^8}{8}\frac{b^2}{16} - \left(de-ac+\frac{cd}{2}\right)\left(\frac{1}{4}+\frac{\beta^2}{2}\ell_n\beta-\frac{\beta^2}{4}\right) - \left(\frac{bc}{2}+\frac{ad}{2}-\frac{d^2}{4}\right)\left(\frac{1}{16}+\frac{\beta^4}{4}\ell_n\beta-\frac{\beta^4}{16}\right) + \frac{d^2}{4}\left[\frac{1}{32}-\frac{\beta^4}{4}(\ell_n\beta)^2+\frac{\beta^4}{8}\ell_n\beta-\frac{\beta^4}{32}\right] - \frac{c^2}{3}(\ell_n\beta)^3 + \frac{bd}{4}\left(\frac{1}{36}+\frac{\beta^6}{6}\ell_n\beta-\frac{\beta^6}{36}\right) - cd\left[\frac{1}{4}-\frac{\beta^2}{2}(\ell_n\beta)^2 + \frac{\beta^2}{2}\ell_n\beta-\frac{\beta^2}{4}\right] + ce(\ell_n\beta)^2 - \left(e^2+4\frac{r_m^{*4}}{B^2}\frac{Br}{\Omega}\right)\ell_n\beta\right\} \quad (33)$$

In many engineering designs and energy optimization problems, the ratio of entropy generation rate caused by heat transfer, N_{HT}, to overall entropy generation rate, N_S, which is known as Bejan number, Be, is needed. The Bejan number is so defined mathematically as

$$Be = \frac{N_{\mathrm{HT}}}{N_S} \quad (34)$$

Clearly, the Bejan number ranges from zero to one. $Be = 0$ is the limit where the irreversibility is dominated by fluid friction effects and $Be = 1$ corresponds to the limit where the irreversibility due to heat transfer by virtue of finite temperature differences dominates. The contributions of both heat transfer and fluid friction to entropy generation are equal when $Be = 1/2$.

III. Results and Discussion

Here, the velocity and temperature profiles are presented as well as the entropy generation number and Bejan number distributions. The results are obtained using $Pr = 0.71$ and $\gamma = 1.4$. Also through this section the values of accommodation coefficients are assumed to be one [38]. Without loss of generality, unless otherwise stated, the results are obtained assuming $Pe^{-2} \to 0$. To validate the analytical solution, a comparison is made between the present results against those of Yari [31] for the special case of the inner wall being adiabatic.

Figure 2 shows dimensionless velocity distribution for different values of Knudsen number at $\beta = 0.3$. As a result of slip conditions, slip velocities occur at both inner and outer walls. An increase in Kn results in an increase in the slip velocities at the walls, while according to mass conservation, the maximum velocity decreases. Because of higher velocity gradients, the slip effect is more pronounced at the inner wall. As expected, the dimensionless velocity distribution is not symmetrical. The maximum velocity occurs close to the inner wall at $r^* = r_m^*$. This is due to the fact that as a result of smaller surface, the momentum exchange between the inner wall and the flow is slighter. Therefore, the fluid particles can take higher velocities near the inner wall. The variation of the maximum velocity point, r_m^*, with the aspect ratio, β, for different values of Knudsen number is shown in Fig. 3. Except for $\beta \to 0$ and $\beta \to 1$, which, respectively, correspond to a circular microchannel and a parallel plate microchannel, increasing values of Knudsen number result in decreasing r_m^*, which means the maximum velocity occurs at a closer point to the inner wall. As noted previously, the slip effect is more pronounced at the inner wall, resulting in more decrease of velocity gradient at the inner wall. Therefore, the ratio of

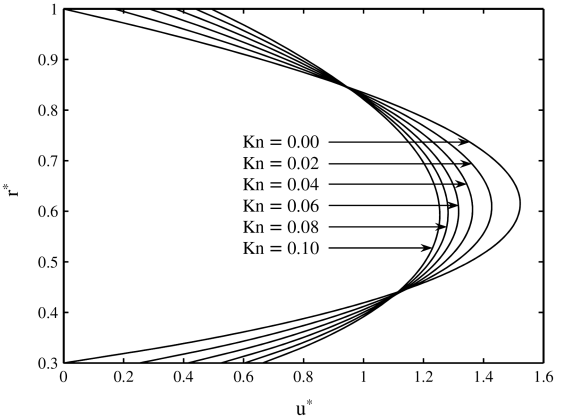

Fig. 2 Transverse distribution of dimensionless velocity for different values of Knudsen number at $\beta = 0.3$.

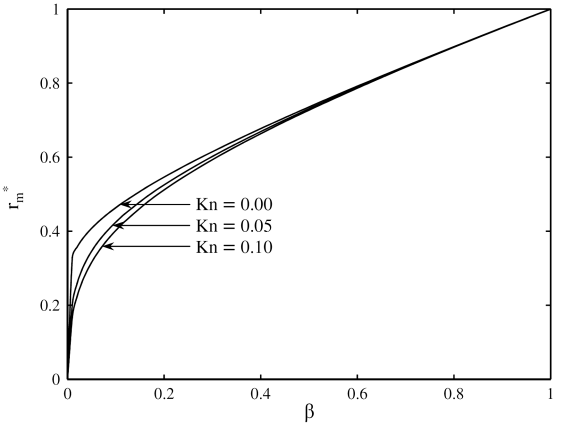

Fig. 3 Variation of r_m^* at different values of Knudsen number.

the inner wall drag to that of the outer wall will be reduced for higher Knudsens, leading to more decrease in the momentum exchange between the inner wall and the flow relative to that for the outer wall. This is why the maximum velocity point shifts to the inner wall. The mechanism of Knudsen number effect on maximum velocity point was found to be based on varying the ratio of the wall drags. Therefore, since for a circular microchannel the inner wall is absent, the Knudsen number has no influence on the maximum velocity point and it occurs at centerline. For a parallel plate, the Knudsen number has similar influences on the both wall drags and as a result, it does not affect the maximum velocity point which is located at centerline.

Figure 4 illustrates the distribution of dimensionless temperature at different values of Brinkman number and the wall heat fluxes ratio for no slip conditions. For each case, both positive and negative values of the wall heat fluxes are considered. Positive values of Brinkman number correspond to the wall cooling case, while the opposite is true for negative values of Brinkman number. For each case, the viscous dissipation behaves like an energy source increasing the temperature of the fluid specially near the walls since higher shear rates occur at these regions, while it is zero at r_m^*. In the absence of viscous dissipation, the distribution of dimensionless temperature is independent of whether the wall is heated or cooled. For symmetric case which corresponds to $\eta = 1$ and for the positive heat fluxes at the walls, the walls temperatures are higher than the bulk temperature. So, increasing viscous dissipation will result in increasing the difference between the wall and the bulk temperature, while the opposite is true for the case with negative wall heat fluxes. For the case of adiabatic inner wall which corresponds to $\eta \to \infty$, the interpretation is more complicated. In this case, for wall cooling, although the temperature of the outer wall is higher than the bulk temperature, but the inner wall temperature is smaller than the bulk

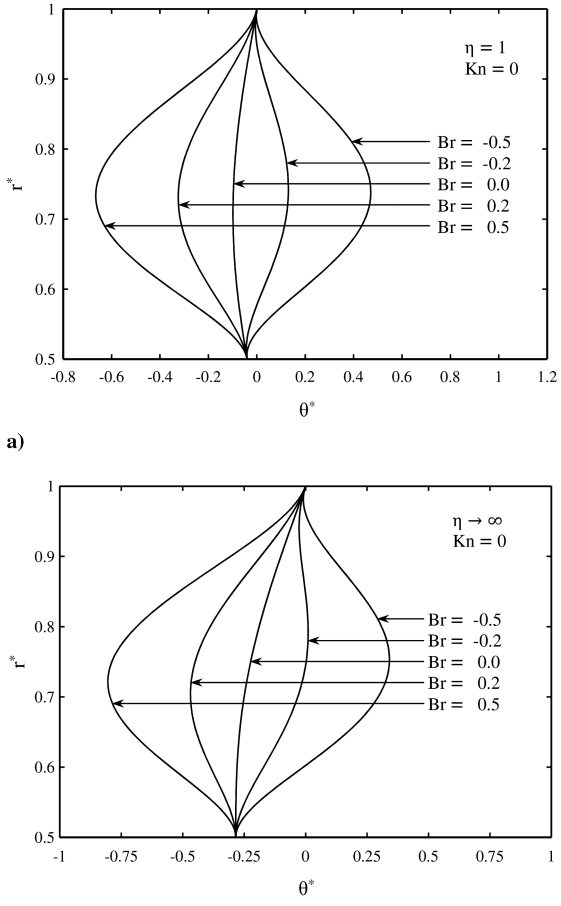

Fig. 4 Transverse distribution of dimensionless temperature at different values of Brinkman number and $\beta = 0.5$: a) $\eta = 1$ and b) $\eta \to \infty$.

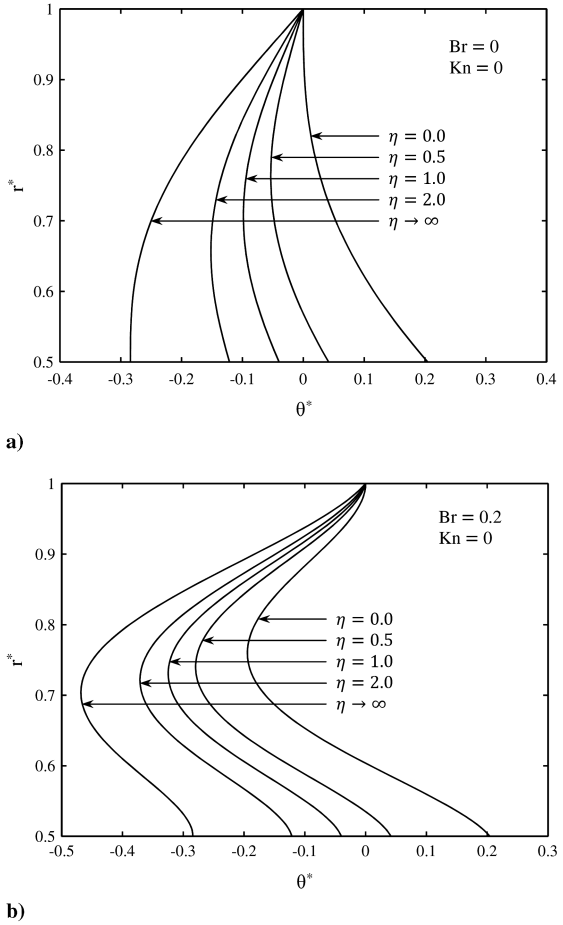

Fig. 5 Transverse distribution of dimensionless temperature for different positive values of η at $\beta = 0.5$: a) $Br = 0$ and b) $Br = 0.2$.

temperature, increasing by viscous heating rather than the bulk temperature. So the difference between the wall and the bulk temperature decreases. It can be deduced that there is a value of η called $\eta_{c,i}$, for which the inner wall temperature is equal to the bulk temperature of fluid. The value of $\eta_{c,i}$ depends on Brinkman and Knudsen numbers as well as the aspect ratio of the annular geometry. At wall cooling case for $\eta_{c,i} < \eta$, the inner wall temperature is smaller than the bulk temperature and vice versa. The corresponding critical value of η for the outer wall is $\eta_{c,o}$. The presence of η_c is more visible in Fig. 5a which shows the distribution of dimensionless temperature at different positive values of η for no slip and no viscous heating case. For $\eta = 0$, the dimensionless temperature of the inner wall is higher than dimensionless bulk temperature, while the opposite is true for $\eta \to \infty$. Comparing the above mentioned case with that including viscous heating which is shown in Fig. 5b reveals that viscous dissipation distorts the profile shapes in a manner that the inner particles take lower values of nondimensional temperature. The temperature distribution in the absence of viscous heating for the case that one wall is cooled while the other is being heated, which is given by Fig. 6a, is quite different from the cases that both walls are being cooled or heated. The main difference is that the minimum values of dimensionless temperature occur at the walls instead of an inner point. Another difference is the nonmonotonic effect of η on the temperature profiles. However, this phenomenon is only due to discontinuity of dimensionless temperature definition at $\eta = -1$ and it is not the result of a physical mechanism. As observed in Fig. 6b, the influence of viscous heating is similar to the case that the heating of both walls are similar. It is worth mentioning that for $\eta = -0.5$, in the absence of viscous heating, the problem is reduced to a conduction heat transfer problem in a long annuli. This can be justified by the fact that as a result of vanishing the axial variation of temperature, no energy is transferred by the flow.

The effect of rarefaction on dimensionless temperature profile is illustrated in Fig. 7. Since in the presence of temperature jump the two dimensionless temperatures given by Eqs. (12) and (26) differ from each other, it is useful to examine the rarefaction effects on the both definitions. Increasing Knudsen number leads to increasing the energy transferred by the flow at the walls and decreasing it in the core region, due to flattening the velocity profile, which this, consequently, leads to decreasing the difference between the temperatures of the inner particles and those located at the walls. The ultimate influence is increasing dimensionless temperature profile based on T_{so}, as observed in Fig. 7a. However, since the temperature jump is increased with increasing values of Knudsen number, the temperature difference between the walls and the fluid particles is strongly increased as well, resulting in decreasing the nondimensional temperature based on T_{wo}. The minimum values of dimensionless temperature occur at a point closer to the inner wall. This is due to the larger surface of the outer wall which leads to a larger influencing domain for the outer wall. The effect of Knudsen number on nondimensional temperature profile based on T_{wo} for $\eta = -2$ is presented in Fig. 8. To increase Knudsen number is to decrease dimensionless temperature as a result of temperature jump at the wall.

Figure 9 shows the distribution of N_S for different values of Br/Ω for symmetric case at no slip conditions. As expected, higher Br/Ω leads to higher N_S due to increasing the fluid friction contribution to entropy generation. Entropy generation number attains its maximum values at the annulus walls due to the presence of high velocity gradients. At $r^* = r_m^*$ at which velocity gradient is zero, the entropy generation number attains its minimum magnitude. The corresponding Bejan number distribution at different values of Br/Ω for the above mentioned case is shown in Fig. 10. For $Br/\Omega = 0$, the fluid friction contribution to entropy generation is zero. Bejan number is independent of radial coordinate and attains its maximum

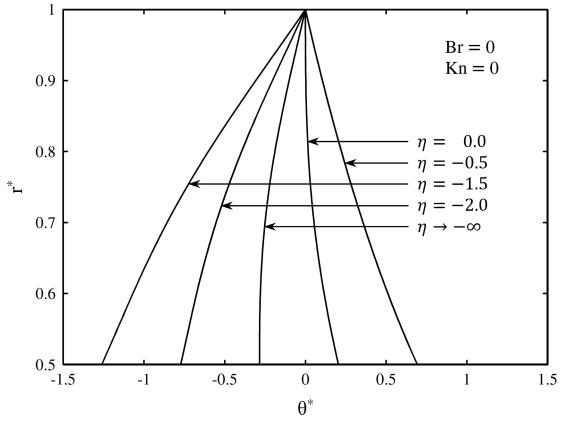

a)

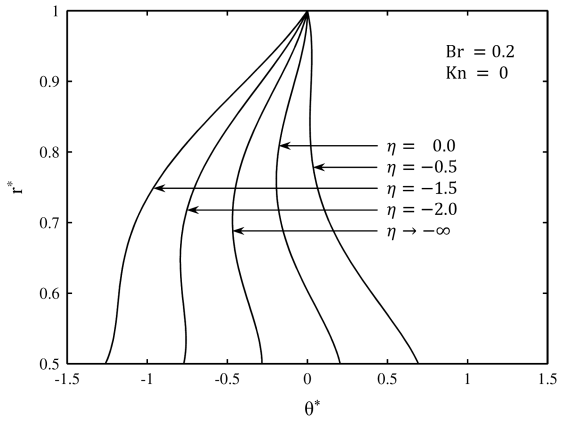

b)

Fig. 6 Transverse distribution of dimensionless temperature for different negative values of η at $\beta = 0.5$: a) $Br = 0$ and b) $Br = 0.2$.

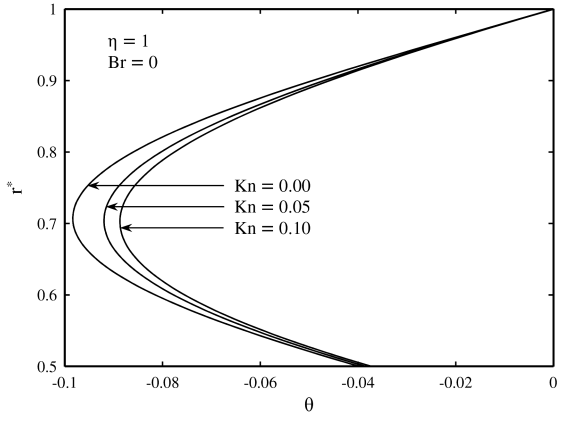

a)

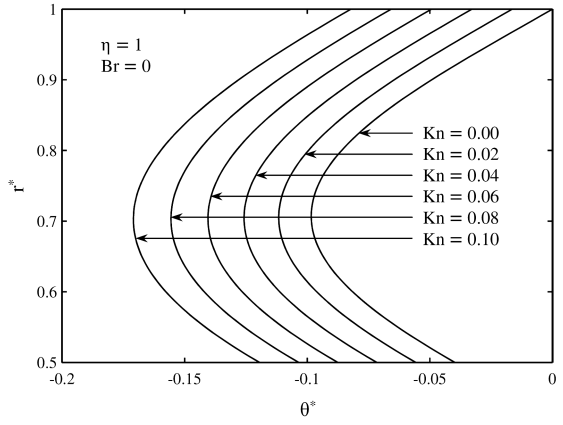

b)

Fig. 7 Effects of rarefaction on dimensionless temperature profile for no viscous heating case with symmetrically heating at $\beta = 0.5$: a) dimensionless temperature based on T_{so} and b) dimensionless temperature based on T_{wo}.

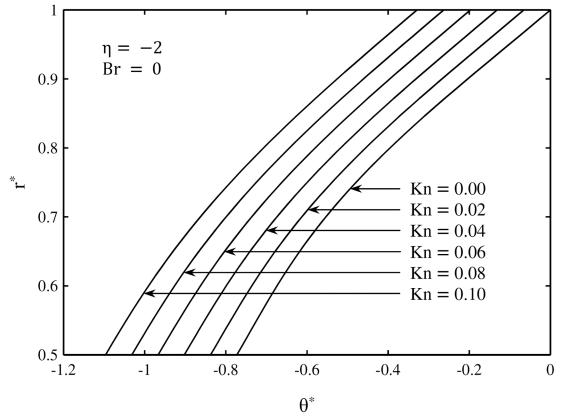

Fig. 8 Effects of rarefaction on dimensionless temperature profile for no viscous heating case at $\eta = -2$ and $\beta = 0.5$.

value which is unity. As Br/Ω increases the Bejan number decreases due to increasing fluid friction effects. The Bejan number is close to zero at the annulus walls, as a result of the high velocity gradient at these regions. As a result of the absence of fluid friction, the Bejan number reaches its maximum value at $r^* = r^*_m$ at which the maximum velocity occurs. Note that the minimum value of Bejan number which is zero, occurs at a point close to the maximum velocity point. This is because for the symmetric case the minimum temperature (note that Br is positive) occurs at a point close to the maximum velocity point.

Figure 11 presents the distribution of N_S for different values of Knudsen number at symmetric case. An increment in Knudsen number leads to a smaller N_S. This is due to the fact that as Knudsen increases the velocity and temperature gradients become smaller. Note that, as mentioned earlier, except for $Br/\Omega = 0$, the minimum N_S occurs at $r^* = r^*_m$. This is due to the fact that fluid friction contribution to entropy generation dominates entropy generation. From Fig. 3 it is clear that although increasing Knudsen number leads to smaller r^*_m, however, the value of Knudsen number does not notably affect the maximum velocity point at $\beta = 0.5$. So, as Knudsen increases the point of minimum N_S shifts slightly to the inner wall. Figure 12 depicts the distribution of Bejan number for two values of Knudsen number at symmetric case. Since at the annulus walls the temperature gradients remain constant, increasing Knudsen leads to higher Be due to decreasing velocity gradients at the walls. For the inner points, as Kn increases Be decreases which implies that the Knudsen number effect on temperature distribution is higher than velocity distribution. The Bejan number has a maximum value at r^*_m and a minimum value at the minimum temperature point which their positions shift to the inner wall for a higher Knudsen number.

The effect of the wall heat fluxes ratio on the entropy generation at no slip conditions is shown in Fig. 13. For positive values of η, an increase in η leads to a higher value of the entropy generation number at the region close to the outer wall, while the opposite is true for the region close to the inner wall. This is due to the fact that according to Fig. 5, as η increases the dimensionless temperature gradient near the outer wall increases, while it decreases near the inner wall. As η increases the minimum point of the entropy generation number, which in this case does not necessarily coincide with r^*_m, shifts to the inner wall. For $\eta = -2$, a different behavior is observed, including a local maximum near the outer wall. Over a wide portion of the cross section, the entropy production related to $\eta = -2$ is the maximum, as a result of higher temperature gradients. The corresponding Bejan number distribution for the above mentioned case is shown in Fig. 14.

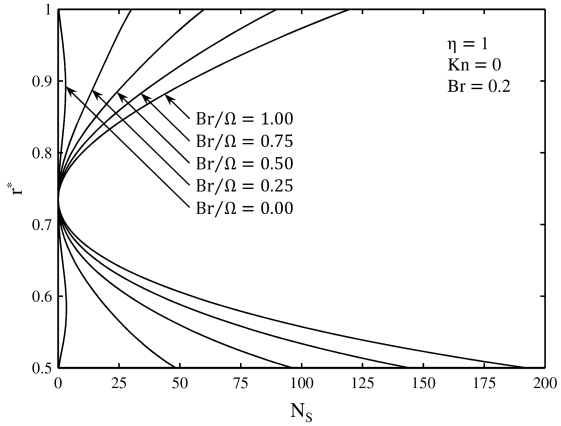

Fig. 9 Transverse distribution of N_S for different values of Br/Ω at $\beta = 0.5$.

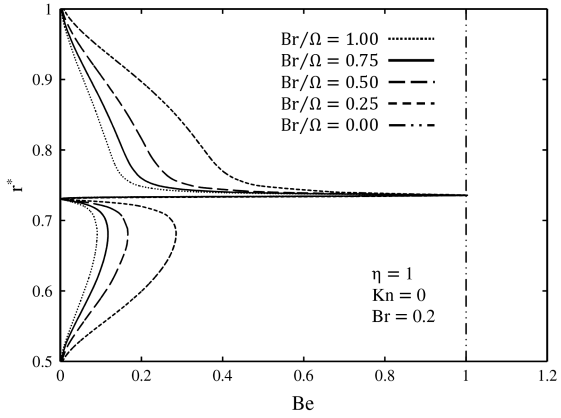

Fig. 10 Transverse distribution of Bejan number for different values of Br/Ω at $\beta = 0.5$.

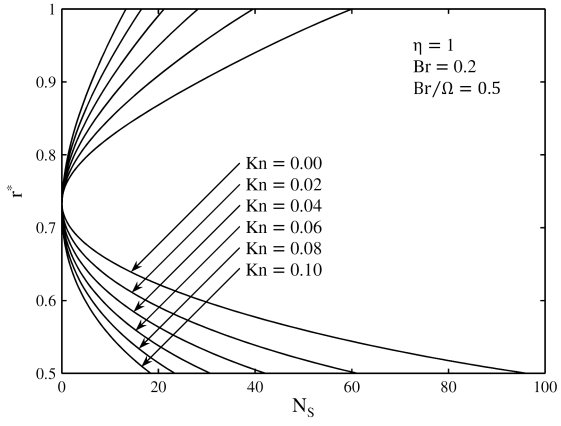

Fig. 11 Distribution of N_S for different values of Knudsen number at $\beta = 0.5$.

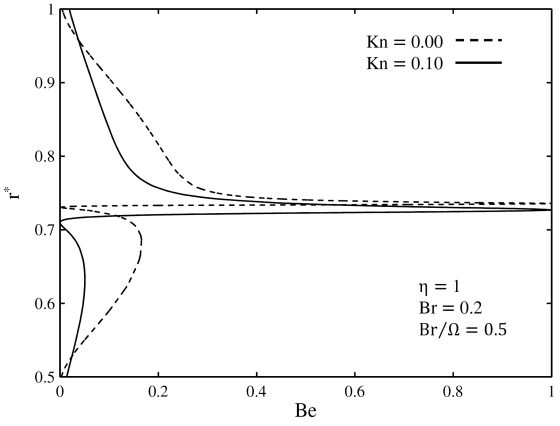

Fig. 12 Distribution of Bejan number for different values of Knudsen number at $\beta = 0.5$.

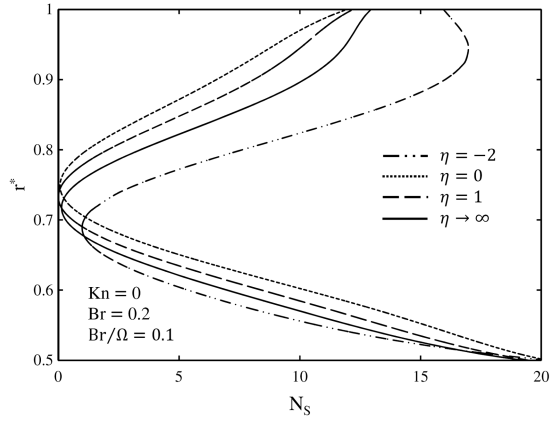

Fig. 13 Distribution of N_S for different values of η at $\beta = 0.5$.

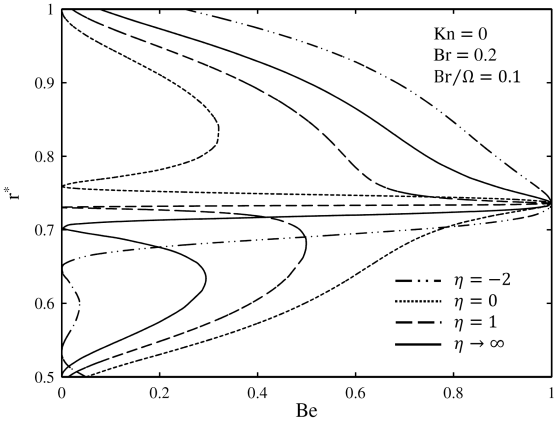

Fig. 14 Distribution of Bejan number for different values of η at $\beta = 0.5$.

Note that since the value of Br/Ω is small, the heat transfer effects are significant. With the exception of $\eta = -2$, a higher value of η leads to higher values of the Bejan number at the region close to the outer wall, while the opposite is true for the region close to the inner wall. The Bejan number for $\eta = -2$ is the maximum near the outer wall, while it is the minimum near the inner wall. Except for $\eta = -2$ which shows two local minimum near the inner wall, since for higher values of the wall heat fluxes ratio the minimum temperature occurs at a closer point to the inner wall, the minimum Bejan number point shifts to the inner wall for higher η, while the maximum Bejan number point remains unchanged.

So far, we have not evaluated the effect of the aspect ratio of annular geometry on entropy generation and have obtained the results using $\beta = 0.5$. Figure 15 illustrates the variation of $N_{S,\mathrm{av}}$ with β at different values of Knudsen number for the special case of the inner wall being adiabatic. Also in this figure a comparison has been made between the present results against those of Yari [31]. It is worth mentioning that when the inner wall is assumed to be adiabatic, the definition of all dimensionless parameters in the present study and those of Yari [31] are the same. As seen, an excellent agreement between the both results is observed. For all Knudsen numbers, as β increases the average entropy generation number severely increases.

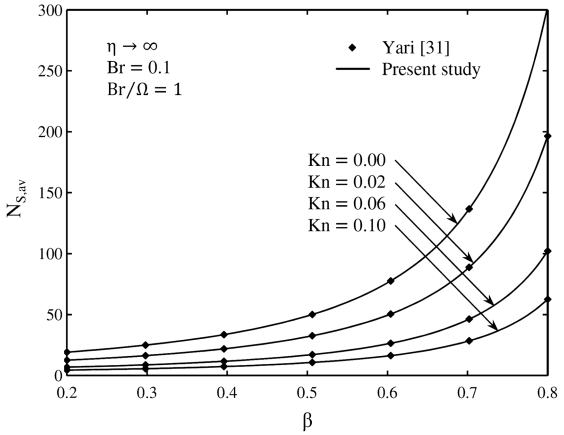

Fig. 15 Variation of $N_{S,av}$ with β at different values of Knudsen number for $\eta \to \infty$.

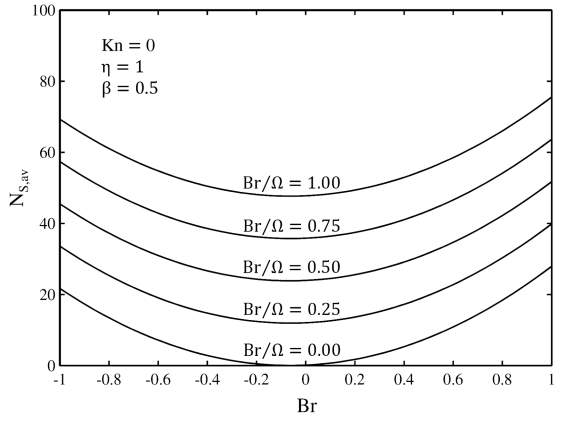

Fig. 17 Variation of $N_{S,av}$ with Br at different values of the group parameter.

This is due to the increase in fluid friction contribution to the entropy generation as a result of the increase in velocity gradients.

The variation of $N_{S,av}$ with the group parameter at different values of the wall heat fluxes ratio is shown in Fig. 16. From Eq. (28) it is clear that the entropy generation is a linear increasing function of Br/Ω, as seen in Fig. 16. With the exception of $\eta = -2$ which is the most irreversible case, increasing η leads to a higher $N_{S,av}$. The entropy generation increment due to increasing η remains constant due to its linear dependency on Br/Ω. So, for large values of the group parameter, the effect of η on entropy generation becomes insignificant. Figure 17 presents the variation of $N_{S,av}$ with Br at different values of Br/Ω. Although the minimum value of $N_{S,av}$ does not exactly occur at $Br = 0$, but roughly speaking, increasing Br with either positive or negative signs leads to higher average entropy generation number.

Figure 18 exhibits the effect of Peclet number on $N_{S,av}$ at different values of η for no slip condition. As observed, higher entropy generation rates are obtained by decreasing Pe. This is because at low Peclet number flows the entropy generation due to axial gradient of temperature distribution becomes important and it is increased by decreasing Pe. In fact, for this kind of flows, the entropy generation is mainly due to axial variations of temperature. At high values of Pe, the axial slope of temperature becomes negligible compared with radial slope and hence the entropy generation takes asymptotic values. Also the results demonstrate that decreasing Pe leads to higher influence of the wall heat fluxes ratio on $N_{S,av}$. Profiles of $N_{S,av}$ merge with each other at high Peclet numbers. The effect of rarefaction on Peclet number dependency of average entropy generation number is illustrated in Fig. 19. The general trend comprising an intense decrease of $N_{S,av}$ for increasing values of Pe until it reaches asymptotic values at high Peclet numbers, is similar

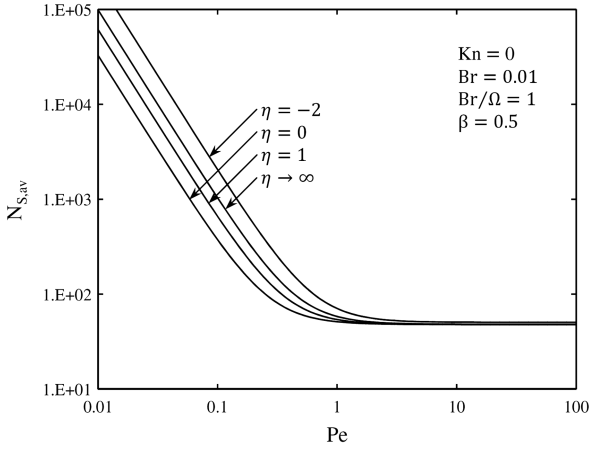

Fig. 18 Average entropy generation number as a function of Peclet number at different values of η.

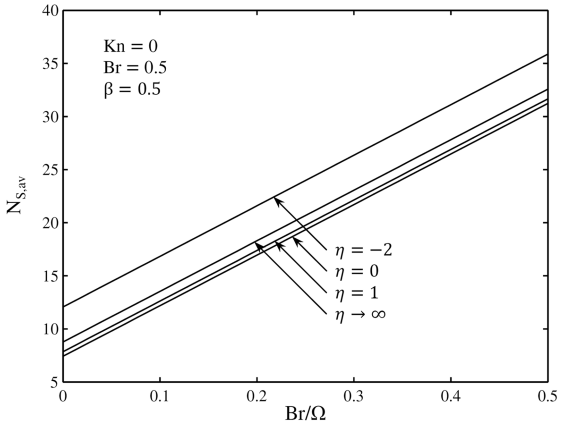

Fig. 16 Variation of $N_{S,av}$ with Br/Ω at different values of η.

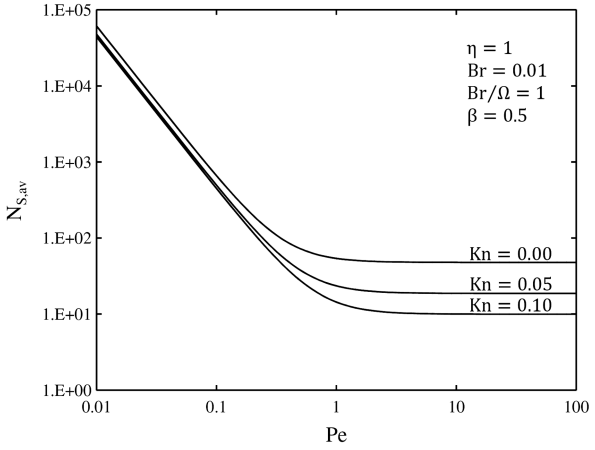

Fig. 19 Average entropy generation number as a function of Peclet number at different Knudsen numbers.

for all Knudsens. For the whole Peclet number domain, to increase Knudsen is to decrease entropy generation. The effects of rarefaction on $N_{S,av}$ is more important at high values of Pe and it becomes slighter at flows having low Peclet numbers.

IV. Conclusions

In the present work, the second law of thermodynamics analysis was carried out for steady-state hydrodynamically- and thermally-fully developed laminar gas flow in a microannulus with constant

wall heat fluxes. The rarefaction effects were taken into consideration using first order slip boundary conditions. Viscous heating was also included for both the wall cooling and the wall heating cases. Using the previously obtained velocity distribution, the energy equation was solved to get the temperature distribution analytically and consequently to compute the entropy generation rates. Some concluding remarks are summarized as follows:

1) The case that one wall is cooled while the other is heated is the most irreversible case. For the case that the both walls are cooled or heated, increasing values of the wall heat fluxes ratio lead to higher entropy generation. However, the influence of the wall heat fluxes ratio on entropy generation is negligible at high values of the group parameter and Peclet number.

2) The effect of increasing values of annulus geometrical aspect ratio is to severely increase entropy generation.

3) The entropy generation decreases as Knudsen number increases. The Knudsen number dependency of entropy generation becomes slighter for low Peclet number flows.

4) The effect of increasing values of Brinkman number and the group parameter is to increase entropy generation.

5) At low Peclet numbers, decreasing Peclet number is accompanied by an intense increase of entropy generation, while for flows having high values of Peclet, it has no effect on entropy generation.

References

[1] Beskok, A., and Karniadakis, G. E., "Simulation of Heat and Momentum Transfer in Complex Micro-Geometries," *Journal of Thermophysics and Heat Transfer*, Vol. 8, No. 4, 1994, pp. 647–655. doi:10.2514/3.594

[2] Liu, J., Tai, Y. C., and Ho, C. M., "MEMS for Pressure Distribution Studies of Gaseous Flows in Microchannels," *Proceedings of IEEE, International Conference on Micro Electro Mechanical Systems*, Amsterdam, The Netherlands, 1995, pp. 209–215.

[3] Hsieh, S. S., Tsai, H. H., Lin, C. Y., Huang, C. F., and Chien, C. M., "Gas Flow in a Long Microchannel," *International Journal of Heat and Mass Transfer*, Vol. 47, Nos. 17–18, 2004, pp. 3877–3887. doi:10.1016/j.ijheatmasstransfer.2004.03.027

[4] Kennard, E. H., *Kinetic Theory of Gases*, McGraw–Hill, New York, 1938.

[5] Ebert, W. A., and Sparrow, E. M., "Slip Flow in Rectangular and Annular Ducts," *Journal of Basic Engineering*, Vol. 87, No. 4, 1965, pp. 1018–1024.

[6] Duan, Z., and Muzychka, Y. S., "Slip Flow in Elliptic Microchannels," *International Journal of Thermal Sciences*, Vol. 46, No. 11, 2007, pp. 1104–1111. doi:10.1016/j.ijthermalsci.2007.01.026

[7] Wang, C. Y., "Slip Flow in Ducts," *Canadian Journal of Chemical Engineering*, Vol. 81, No. 5, 2003, pp. 1058–1061.

[8] Bahrami, M., Tamayol, A., and Taheri, P., "Slip-Flow Pressure Drop in Microchannels of General Cross Section," *Journal of Fluids Engineering*, Vol. 131, No. 3, 2009, p. 031201. doi:10.1115/1.3059699

[9] Zhang, T. T., Jia, L., Wang, Z. C., and Li, X., "The Application of Homotopy Analysis Method for 2-Dimensional Steady Slip Flow in Microchannels," *Physics Letters A*, Vol. 372, No. 18, 2008, pp. 3223–3227. doi:10.1016/j.physleta.2008.01.077

[10] Zhang, T. T., Jia, L., Wang, Z. C., and Li, C. W., "Slip Flow Characteristics of Compressible Gaseous in Microchannels," *Energy Conversion and Management*, Vol. 50, No. 7, 2009, pp. 1676–1681. doi:10.1016/j.enconman.2009.03.032

[11] Ameel, T. A., Wang, X. M., Baron, R. F., and Warrington, R. O., "Laminar Forced Convection in a Circular Tube with Constant Heat Flux and Slip Flow," *Microscale Thermophysical Engineering*, Vol. 1, No. 4, 1997, pp. 303–320. doi:10.1080/108939597200160

[12] Zhu, X., Xin, M. D., and Liao, Q., "Analysis of Heat Transfer Between Two Unsymmetrically Heated Parallel Plates with Microspacing in the Slip Flow Regime," *Microscale Thermophysical Engineering*, Vol. 6, No. 4, 2002, pp. 287–301. doi:10.1080/10893950290098311

[13] Zhang, T. T., Jia, L., Wang, Z. C., Li, C. W., and Jaluria, Y., "Fluid Heat Transfer Characteristics with Viscous Heating in the Slip Flow Region," *Europhysics Letters*, Vol. 85, No. 4, 2009, p. 40006. doi:10.1209/0295-5075/85/40006

[14] Duan, Z., and Muzychka, Y. S., "Slip Flow Heat Transfer in Annular Microchannels with Constant Heat Flux," *Journal of Heat Transfer*, Vol. 130, No. 9, 2008, p. 092401. doi:10.1115/1.2946474

[15] Avci, M., and Aydin, O., "Laminar Forced Convection Slip-Flow in a Micro-Annulus Between Two Concentric Cylinders," *International Journal of Heat and Mass Transfer*, Vol. 51, Nos. 13–14, 2008, pp. 3460–3467. doi:10.1016/j.ijheatmasstransfer.2007.10.036

[16] Tunc, G., and Bayazitoglu, Y., "Heat Transfer in Rectangular Microchannels," *International Journal of Heat and Mass Transfer*, Vol. 45, No. 4, 2002, pp. 765–773. doi:10.1016/S0017-9310(01)00201-0

[17] Hooman, K., "A Superposition Approach to Study Slip-Flow Forced Convection in Straight Microchannels of Uniform but Arbitrary Cross-Section," *International Journal of Heat and Mass Transfer*, Vol. 51, Nos. 15–16, 2008, pp. 3753–3762. doi:10.1016/j.ijheatmasstransfer.2007.12.014

[18] Khan, W. A., and Yovanovich, M. M., "Analytical Modeling of Fluid Flow and Heat Transfer in Microchannel/Nanochannel Heat Sinks," *Journal of Thermophysics and Heat Transfer*, Vol. 22, No. 3, 2008, pp. 352–359. doi:10.2514/1.35621

[19] Hooman, K., Hooman, F., and Famouri, M., "Scaling Effects for Flow in Micro-Channels: Variable Property, Viscous Heating, Velocity Slip, and Temperature Jump," *International Communications in Heat and Mass Transfer*, Vol. 36, No. 2, 2009, pp. 192–196. doi:10.1016/j.icheatmasstransfer.2008.10.003

[20] Sadeghi, A., Asgarshamsi, A., and Saidi, M. H., "Analysis of Laminar Flow in the Entrance Region of Parallel Plate Microchannels for Slip Flow," *Proceedings of the Seventh International ASME Conference on Nanochannels, Microchannels and Minichannels, ICNMM2009*, Pohang, South Korea, 2009.

[21] Chen, C. K., and Weng, H. C., "Natural Convection in a Vertical Microchannel," *Journal of Heat Transfer*, Vol. 127, No. 9, 2005, pp. 1053–1056. doi:10.1115/1.1999651

[22] Weng, H. C., and Chen, C. K., "On the Importance of Thermal Creep in Natural Convective Gas Microflow with Wall Heat Fluxes," *Journal of Physics D: Applied Physics*, Vol. 41, No. 11, 2008, p. 115501. doi:10.1088/0022-3727/41/11/115501

[23] Weng, H. C., and Chen, C. K., "Variable Physical Properties in Natural Convective Gas Microflow," *Journal of Heat Transfer*, Vol. 130, No. 8, 2008, p. 082401. doi:10.1115/1.2927400

[24] Biswal, L., Som, S. K., and Chakraborty, S., "Effects of Entrance Region Transport Processes on Free Convection Slip Flow in Vertical Microchannels with Isothermally Heated Walls," *International Journal of Heat and Mass Transfer*, Vol. 50, Nos. 7–8, 2007, pp. 1248–1254. doi:10.1016/j.ijheatmasstransfer.2006.09.025

[25] Chakraborty, S., Som, S. K., and Rahul, "A Boundary Layer Analysis for Entrance Region Heat Transfer in Vertical Microchannels Within the Slip Flow Regime," *International Journal of Heat and Mass Transfer*, Vol. 51, Nos. 11–12, 2008, pp. 3245–3250. doi:10.1016/j.ijheatmasstransfer.2008.01.019

[26] Bejan, A., "Second-Law Analysis in Heat Transfer and Thermal Design," *Advances in Heat Transfer*, Vol. 15, 1982, pp. 1–58.

[27] Bejan, A., *Entropy Generation Minimization*, CRC Press, New York, 1996.

[28] Haddad, O., Abuzaid, M., and Al-Nimr, M., "Entropy Generation due to Laminar Incompressible Forced Convection Flow Through Parallel Plates Microchannel," *Entropy*, Vol. 6, No. 5, 2004, pp. 413–426. doi:10.3390/e6050413

[29] Avci, M., and Aydin, O., "Second Law Analysis of Heat and Fluid Flow in Microscale Geometries," *International Journal of Exergy*, Vol. 4, No. 3, 2007, pp. 286–301. doi:10.1504/IJEX.2007.013395

[30] Hooman, K., "Entropy Generation for Microscale Forced Convection: Effects of Different Thermal Boundary Conditions, Velocity Slip, Temperature Jump, Viscous Dissipation, and Duct Geometry," *International Communications in Heat and Mass Transfer*, Vol. 34, No. 8, 2007, pp. 945–957. doi:10.1016/j.icheatmasstransfer.2007.05.019

[31] Yari, M., "Second Law Analysis of Flow and Heat Transfer Inside a Microannulus," *International Communications in Heat and Mass Transfer*, Vol. 36, No. 1, 2009, pp. 78–87. doi:10.1016/j.icheatmasstransfer.2008.09.003

[32] Adams, T. M., Abdel-Khalik, S. I., Jeter, S. M., and Qureshi, Z. H., "An Experimental Investigation of Single Phase Forced Convection in Microchannels," *International Journal of Heat and Mass Transfer*, Vol. 41, Nos. 6–7, 1998, pp. 851–857. doi:10.1016/S0017-9310(97)00180-4

[33] Beskok, A., Karniadakis, G. E., and Trimmer, W., "Rarefaction and Compressibility Effects in Gas Microflows," *Journal of Fluids Engineering*, Vol. 118, No. 3, 1996, pp. 448–456. doi:10.1115/1.2817779

[34] Schaaf, S. A., "Mechanics of Rarefied Gases," *Fluid Dynamics 2*, Encyclopedia of Physics, Vol. 8.2, Springer–Verlag, Berlin, 1963, pp. 591–624.

[35] Sharipov, F., and Seleznev, V., "Data on Internal Rarefied Gas Flows," *Journal of Physical and Chemical Reference Data*, Vol. 27, No. 3, 1998, pp. 657–706.

[36] Hadjiconstantinou, N. G., "The Limits of Navier–Stokes Theory and Kinetic Extensions for Describing Small Scale Gaseous Hydrodynamics," *Physics of Fluids*, Vol. 18, No. 11, 2006, p. 111301. doi:10.1063/1.2393436

[37] Bejan, A., "The Thermodynamic Design of Heat and Mass Transfer Processes and Devices," *International Journal of Heat and Fluid Flow*, Vol. 8, No. 4, 1987, pp. 258–276. doi:10.1016/0142-727X(87)90062-2

[38] Barron, R. F., Wang, X., Ameel, T. A., and Warrington, R. O., "The Graetz Problem Extended to Slip Flow," *International Journal of Heat and Mass Transfer*, Vol. 40, No. 8, 1997, pp. 1817–1823. doi:10.1016/S0017-9310(96)00256-6